Computers and Geosciences 111 (2018) 26–38

Contents lists available at ScienceDirect

Computers and Geosciences

journal homepage: www.elsevier.com/locate/cageo

Research paper

Method based on the Laplace equations to reconstruct the river terrain for two-dimensional hydrodynamic numerical modeling

Ruixun Lai *, Min Wang, Ming Yang, Chao Zhang

Yellow River Institute of Hydraulic Research, Zhengzhou, 450003, China

ARTICLE INFO

Keywords:
Laplace equations
River terrain model
2D shallow-water equations
Streamlines

ABSTRACT

The accuracy of the widely-used two-dimensional hydrodynamic numerical model depends on the quality of the river terrain model, particularly in the main channel. However, in most cases, the bathymetry of the river channel is difficult or expensive to obtain in the field, and there is a lack of available data to describe the geometry of the river channel. We introduce a method that originates from the grid generation with the elliptic equation to generate streamlines of the river channel. The streamlines are numerically solved with the Laplace equations. In the process, streamlines in the physical domain are first computed in a computational domain, and then transformed back to the physical domain. The interpolated streamlines are integrated with the surrounding topography to reconstruct the entire river terrain model. The approach was applied to a meandering reach in the Qinhe River, which is a tributary in the middle of the Yellow River, China. Cross-sectional validation and the two-dimensional shallow-water equations are used to test the performance of the river terrain generated. The results show that the approach can reconstruct the river terrain using the data from measured cross-sections. Furthermore, the created river terrain can maintain a geometrical shape consistent with the measurements, while generating a smooth main channel. Finally, several limitations and opportunities for future research are discussed.

1. Introduction

In numerical hydrodynamic models, which are major tools for flood simulation and are widely applied in hydraulic engineering and flood risk analysis, the bathymetry of the computational domain is obtained from the river terrain model whose quality significantly affects the accuracy of the simulated water level, velocity and bed deformation (Hardy et al., 1999; Horritt et al., 2006; Raber et al., 2007; Podhornyi et al., 2013). The river terrain model of a computational domain can be divided into two parts. The first part is the floodplain area, where topographical data can be acquired using conventional techniques, such as LiDAR (Light Detection And Ranging) or photogrammetry (Li et al., 2005). Within the floodplain, the elevation points or contour lines are the commonly-used data type to represent topography. The second part of the river terrain is the area covered by water, where the river bathymetry is difficult or expensive to obtain using traditional remote sensing techniques.

There are three widely-used methods to acquire river bathymetry. A direct method is to measure the water depth at a sufficient number of points, and to generate the terrain of the entire domain using classical spatial interpolation methods (Jansen, 1979), with commonly-used methods including IDW (inverse distance weighting), NN (nearest neighbor), and OK (ordinary kriging) interpolation (Li and Heap, 2011). The direct method has been very successful for large domains, such as in a coastal terrain (Bailly du Bois, 2011; Vogel and Mrker, 2010). In these cases, the historical dataset and the newly-acquired sample points are used to rebuild the terrain of the study area. However, in most cases, historical data concerning the geometry of the river is scarce, with cross-sections often the only data source, making the interpolation of high-quality data for the river bathymetry difficult to realize (Schppi et al., 2010).

A second method is the use of advanced instruments, such as ship-based multi-beam SoNARs (Sound Navigation and Ranging), which are also known as multi-beam echo-sounders. These are widely applied for bathymetry mapping of the seafloor and rivers (Intelmann, 2006; Nittrouer et al., 2008; Colbo et al., 2014). The multi-beam SoNAR is an active remote sensing system that provides data of the topography of a riverbed for generating spatially smooth and high-resolution topographical data. The limitation of the multi-beam SoNAR system occurs in shallow-water environments, where seamless data between a water body and dry land is difficult to realize (Costa et al., 2009). Moreover, it is an expensive method for obtaining river bathymetry.

The third method interpolates data from measured cross-sections to

* Corresponding author.
E-mail address: lairuixun@163.com (R. Lai).

https://doi.org/10.1016/j.cageo.2017.10.006
Received 18 December 2016; Received in revised form 26 September 2017; Accepted 11 October 2017
Available online 14 October 2017

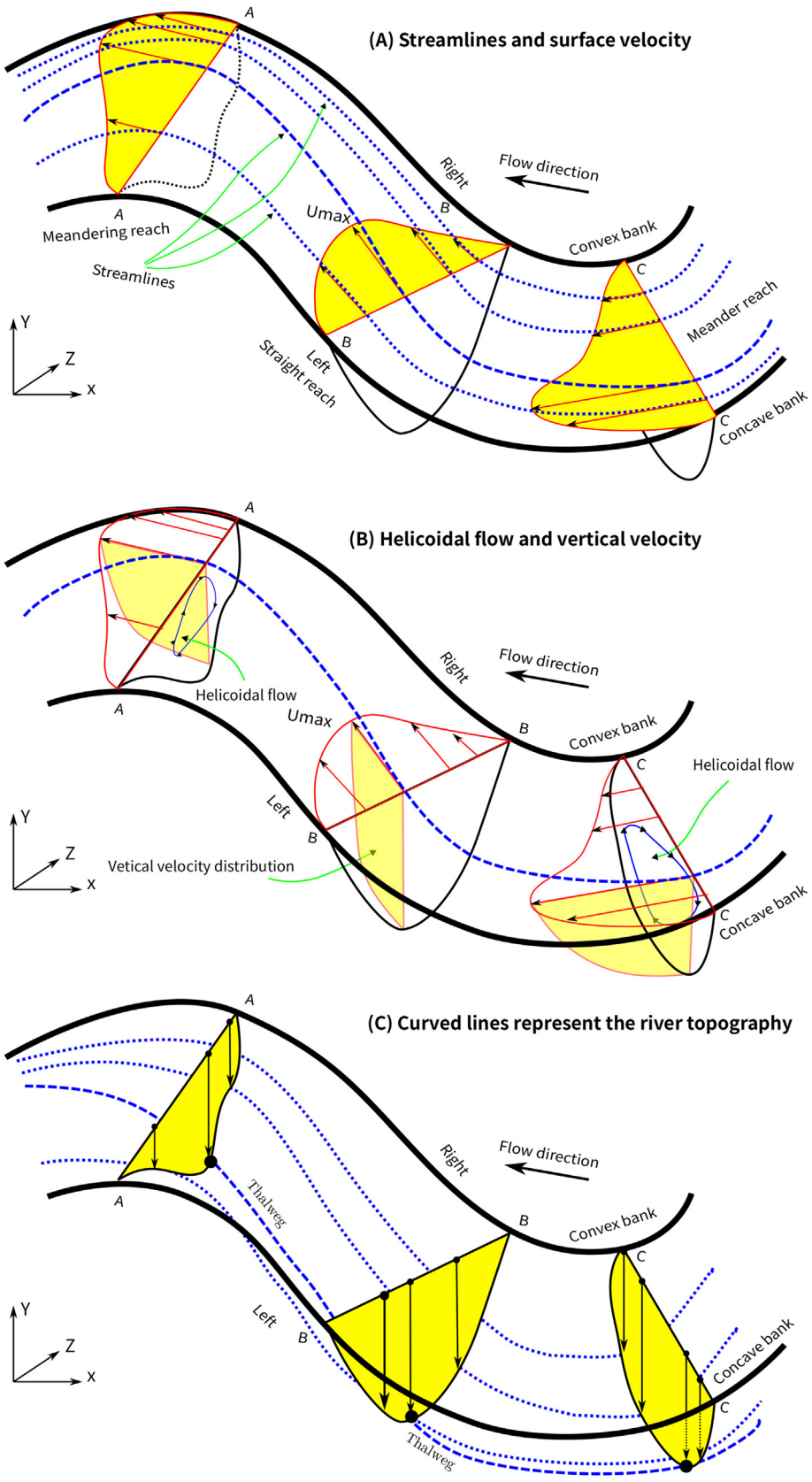

Fig. 1. General idea of reconstructing the river topography.

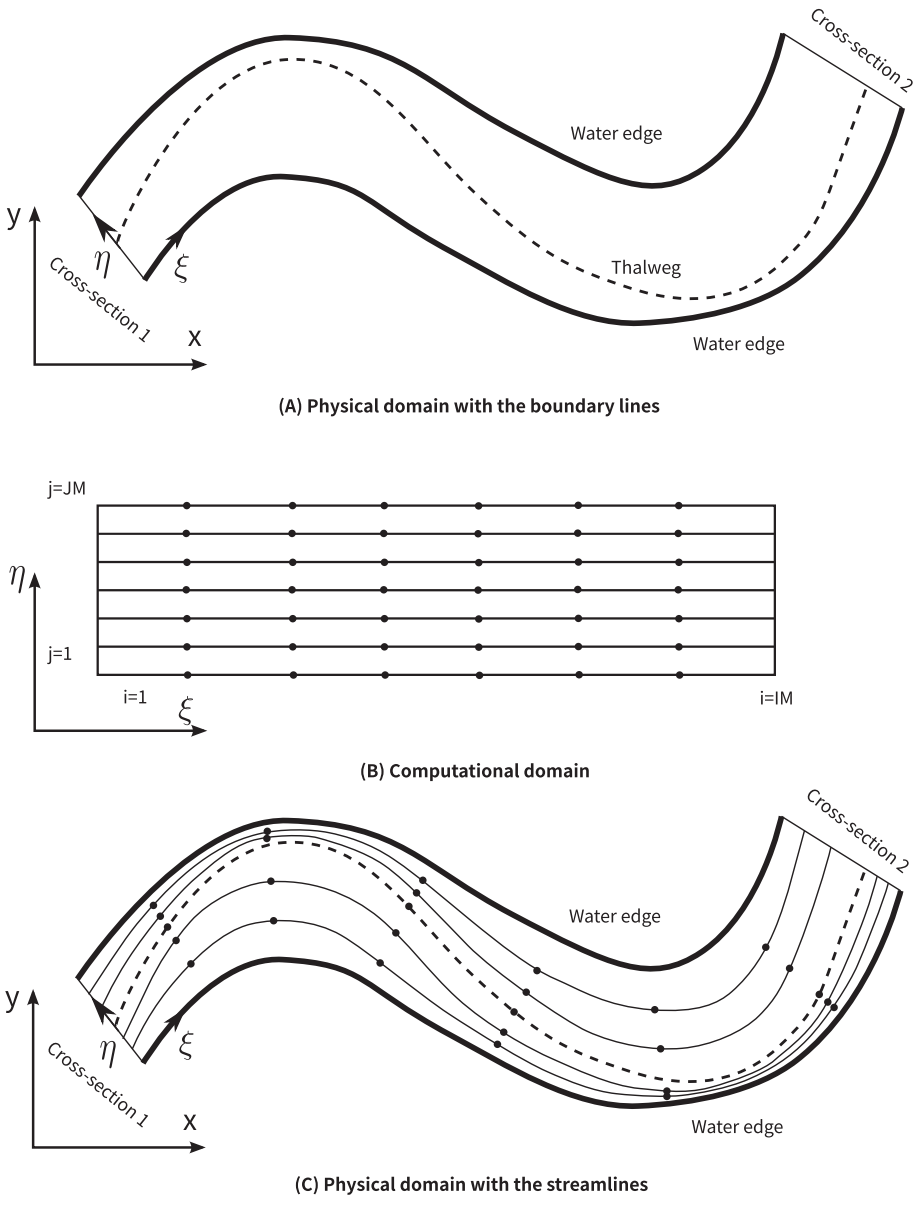

Fig. 2. Description of streamline generation.

reconstruct the river channel terrain. While the practical application of a hydrodynamical numerical model requires that some historical data be used to validate the parameters in the model, in most cases, the cross-section data are the only geometric data source of the river channel. However, using cross-section data to rebuild the topography of the riverbed has proved to be effective, and thus has received much attention in recent years.

For example (Merwade et al., 2005, 2008), introduced a curvilinear orthogonal coordinate to reference data along the river flow, and to generate three-dimensional topographic data of river channels. This interpolation method was used to create a three-dimensional mesh for the main channel, and to integrate it with the surrounding topography (Schppi et al., 2010). combined lateral river profiles with a digital terrain model to produce a grid, and interpolated cross-section data to the grid points to improve the terrain quality (Caviedes-Voullime et al., 2014). used splines to interpolate cross-section data in the horizontal plane and the vertical direction for which the elevation was obtained by interpolating along the bank, thalweg and interior splines.

We introduce a new algorithm here to reconstruct the river terrain model from the measured cross-sectional data and floodplain topography, and to build a two-dimensional hydrodynamic numerical model. The streamlines of the river channel are created based on the idea of structured grid generation. After the elevations of vertices along the streamlines are interpolated using measured cross-sections, the streamlines are interpolated with the surrounding contour lines to obtain the whole river terrain model. The advantages of this method are that the generated streamlines, which are constrained by the Laplace equations over the whole region, fit well with the curved boundary of the river bank and do not intersect each other.

The next section reviews the river morphology, and introduces the main idea for reconstructing the river terrain model. The method using the Laplace equations to generate the streamlines in the river channel is provided in Section 3. In Section 4, a reach in the Qinhe River is taken as an example to demonstrate the proposed method. The application results and validation are also presented in Section 4. Finally, the conclusions and future lines of research are provided in Section 5.

2. General idea of reconstructing the river terrain

Understanding the general river morphology is the first step in

reconstructing the river terrain. The morphology of a river focuses on the structure and form of the river, which includes the river pattern, channel geometry, profile and velocity distribution. The morphology of a river is the result of several variables and their interactions, which can be categorized as the hydraulics of the flow (e.g., velocity, discharge, roughness and bed shear), channel configurations (e.g., width, depth, shape, and slope) and upstream load (e.g., sediment and discharge) (Marie Morisawa and Clayton, 1985).

For natural rivers, the river pattern is used to describe the plan view of a reach, and includes straight, meandering and braiding (Leopold and Wolman, 1957). While straight and meandering rivers have similar river morphologies, straight rivers have negligible sinuosity in the bankfull stage, whereas meandering rivers have unstable channels with bends (Petersen, 1986). A braiding river has numerous channels that divide and rejoin in braided reaches.

Fig. 1(A) shows a hypothetical river with straight and meandering reaches. On the surface of the flow, a streamline of maximum velocity represents the maximum vertical average velocity along the river channel and divides the streamlines into two parts. The streamline of maximum velocity is nearer the concave bank of each bend and crosses over near the point of inflection between the banks (Morisawa, 1968).

The flow at a river bend produces a super-elevation of the water surface at the concave bank and a lower water surface at the convex bank. At the bends, the vertical velocity and transverse velocity simultaneously affect the riverbed. On the bed, the distribution of the vertical velocity is similar but smaller than the surface velocity. The transverse velocity, or helicoidal flow, can transfer the bed load from the concave bank toward the convex bank, as shown in Fig. 1(B). Thus, the concave bank of the bend is constantly eroding, whereas deposition occurs on the convex bank. Moreover, the cross-section in the bend is triangular with the highest water depth near the concave bank.

On the riverbed, the thalweg is a line representing the lowest elevation along the river channel. Similar to the streamline of maximum velocity on the water surface, the path of the thalweg is closer to the concave banks and crosses over from one bank to the other downstream (Fig. 1(C)).

One can imagine that other curved lines at both sides of the thalweg on the riverbed can be applied to represent the bathymetry of the main channel. These curved lines on the bed are identified by two planes. In the horizontal plane, the curved lines are similar to the streamlines on the surface, concentrate at the concave bank, and disperse at the convex bank. In the vertical plane, these curved lines intersect with the measured cross-sections and can interpolate their elevations at the vertices. The elevations value of the other vertices between cross-sections able to be linearly interpolated. Thus, the key to reconstructing the river topography is the generation of the streamlines using the path of the thalweg and measured cross-sections.

3. Description the river terrain model

3.1. Mathematical foundation for the generation of the streamlines

Based on the morphology of a river, we use the Laplace equations to generate the streamlines in the river channel. The general idea for generating the streamlines of the riverbed originates from the specification of the numerical grid using the elliptic equations first introduced by (Thompson et al., 1985). Grid generation based on the elliptic equations is an advanced algorithm for obtaining a structured mesh, and has many applications in the field of computational fluid dynamics (Fletcher and Srinivas, 1991; Anderson, 1995). For this type of algorithm, the form of the Laplace or Poisson equation is applied to solve the coordinates of the grid points in the physical domain, with the advantage that the generated mesh performs a so-called body-fitted boundary. This preserves the shape of the physical domain, and is useful to generate the streamlines of the naturally curved boundary of rivers.

To apply the Laplace-equation-based grid-generation method to obtain the streamlines, some adjustments and simplifications have been considered. The adjustment is that the water edge at both banks is considered to be the outer boundary, while the thalweg line is taken as the inner boundary. The simplification is that only the grid lines along the channel direction are used to obtain the curved lines, whereas the grid lines across the river are ignored.

Fig. 2 illustrates the generation of the riverbed streamlines. Supposing that some general boundary lines of a river channel have been provided, including the water edge and the thalweg, which are given in x and y coordinates, the problem of generating the vertices of the streamlines can be considered as a boundary-value problem in the physical domain. This process may be solved using the Laplace equations to locate the coordinates of the interior points (Fig. 2(A)).

The simplest elliptic partial differential equations are the Laplace equations, which are described in two-dimensional space as

$$\frac{\partial^2 \xi}{\partial x^2} + \frac{\partial^2 \xi}{\partial y^2} = 0 \tag{1}$$

$$\frac{\partial^2 \eta}{\partial x^2} + \frac{\partial^2 \eta}{\partial y^2} = 0 \tag{2}$$

where x and y represent the coordinates in the physical domain, and ξ and η refer to the points in the computational domain. Equations (1) and (2) can be solved using iterative techniques such as Gauss-Seidel iteration or successive over relaxation (Knabner and Angermann, 2003). When using the finite-difference scheme to solve the equations, the process must occur in a rectangular domain with uniform grid spacing. To transform the boundaries from the physical domain to a rectangular domain (which is called a computational domain), one can imagine that the boundaries are twisted and stretched, as shown in Fig. 2(B). Mathematical expressions to describe this transformation is by interchanging the independent and dependent variables in Equations (1) and (2), whose mathematical proof is given by (Thompson et al., 1977). With the transformation, the Laplace Equations (1) and (2) become

$$\alpha \frac{\partial^2 x}{\partial \xi^2} - 2\beta \frac{\partial^2 x}{\partial \xi \partial \eta} + \gamma \frac{\partial^2 x}{\partial \eta^2} = 0 \tag{3}$$

$$\alpha \frac{\partial^2 y}{\partial \xi^2} - 2\beta \frac{\partial^2 y}{\partial \xi \partial \eta} + \gamma \frac{\partial^2 y}{\partial \eta^2} = 0 \tag{4}$$

where

$$\alpha = \left(\frac{\partial x}{\partial \eta}\right)^2 + \left(\frac{\partial y}{\partial \eta}\right)^2 \tag{5}$$

$$\beta = \frac{\partial x}{\partial \xi}\frac{\partial x}{\partial \eta} + \frac{\partial y}{\partial \xi}\frac{\partial y}{\partial \eta} \tag{6}$$

$$\gamma = \left(\frac{\partial x}{\partial \xi}\right)^2 + \left(\frac{\partial y}{\partial \xi}\right)^2 \tag{7}$$

The system of Laplace Equations (3) and (4) is solved in the computational domain (ξ, η) to provide the grid point locations in the physical domain (x, y) (Fig. 2(C)).

3.2. Numerical solution for the streamlines

The numerical solution of Equations (3) and (4) are discretized using a finite-difference scheme following a second-order central-difference approximation:

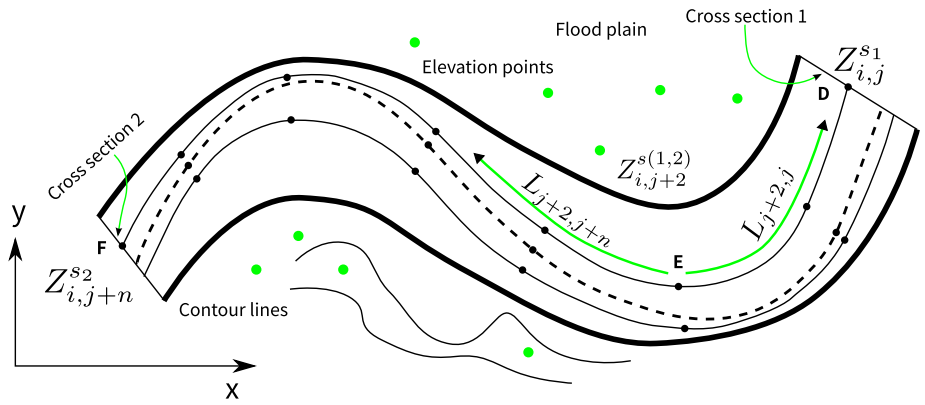

Fig. 3. Interpolation of the elevation of the river bed.

$$\alpha\left[\frac{x_{i+1,j}-2x_{i,j}+x_{i-1,j}}{(\Delta\xi)^2}\right]-2\beta\left[\frac{x_{i+1,j+1}-x_{i+1,j-1}+x_{i-1,j-1}-x_{x-1,j+1}}{4\Delta\xi\Delta\eta}\right]+\gamma\left[\frac{x_{i,j+1}-2x_{i,j}+x_{i,j-1}}{(\Delta\eta)^2}\right]=0 \tag{8}$$

$$\alpha\left[\frac{y_{i+1,j}-2x_{i,j}+y_{i-1,j}}{(\Delta\xi)^2}\right]-2\beta\left[\frac{y_{i+1,j+1}-y_{i+1,j-1}+y_{i-1,j-1}-y_{x-1,j+1}}{4\Delta\xi\Delta\eta}\right]+\gamma\left[\frac{y_{i,j+1}-2y_{i,j}+y_{i,j-1}}{(\Delta\eta)^2}\right]=0 \tag{9}$$

In general, the methods to solve Equations (8) and (9) can be classified as either direct or iterative. The most common direct methods are Cramer's rule and Gaussian elimination, which require an enormous amount of arithmetic operations, and are limited by the size of the coefficient matrix, the storage requirements or programming difficulty. Therefore, iterative methods are widely used because the iterative procedures used to solve a set of linear algebraic equations are easy to program. These methods use initially guessed or previously computed values to solve the dependent variables at each grid point, and then repeated until a specified convergence criterion is reached.

The Gauss-Seidel iteration method is a commonly-used iterative algorithm, whereby the newly computed values of the dependent variables are used to compute the neighboring points when available, with the advantage of an increase in the convergence rate and much less computational time. The Gauss-Seidel scheme of Equations (8) and (9) is described as:

$$2\left[\frac{\alpha}{(\Delta\xi)^2}+\frac{\gamma}{(\Delta\eta)^2}\right]x_{i,j}=\frac{\alpha}{(\Delta\xi)^2}\left[x_{i+1,j}+x_{i-1,j}\right]+\frac{\gamma}{(\Delta\eta)^2}\left[x_{i,j+1}+x_{i,j-1}\right]-\frac{\beta}{2\Delta\xi\Delta\eta}\left[x_{i+1,j+1}-x_{i+1,j-1}+x_{i-1,j-1}-x_{i-1,j+1}\right] \tag{10}$$

$$2\left[\frac{\alpha}{(\Delta\xi)^2}+\frac{\gamma}{(\Delta\eta)^2}\right]y_{i,j}=\frac{\alpha}{(\Delta\xi)^2}\left[y_{i+1,j}+y_{i-1,j}\right]+\frac{\gamma}{(\Delta\eta)^2}\left[y_{i,j+1}+y_{i,j-1}\right]-\frac{\beta}{2\Delta\xi\Delta\eta}\left[y_{i+1,j+1}-y_{i+1,j-1}+y_{i-1,j-1}-y_{i-1,j+1}\right] \tag{11}$$

To initiate the calculation, an initial distribution of x and y coordinates of the grid points in the physical domain must first be obtained from an algebraic model in the computational domain. For example, the grid points can be uniformly packed along the boundaries in the computational domain. The coefficients α, β and γ in Equations (10) and (11) are determined from Equations (5)–(7) using finite-difference approximations. For the first iteration, the x and y values are given by the initial guessed values. In the next iteration, the values of the variables are replaced by the previous iteration, and repeated until a specified

Fig. 4. Location of the Shuibeicun reach.

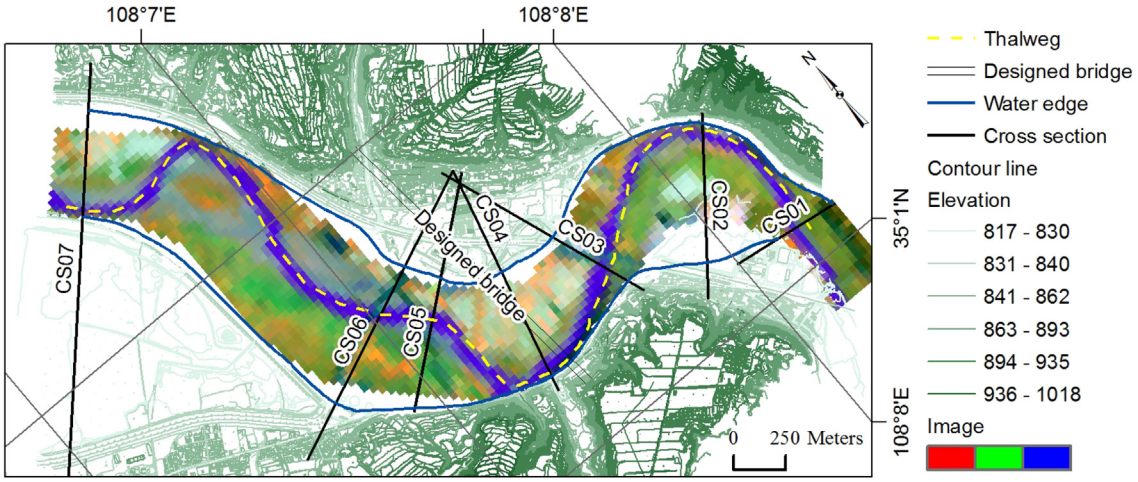

Fig. 5. The river terrain inferred from measurements.

Table 1
Locations of the intersection points between the water surface profile and the cross-sections.

No. of cross-section	Water surface	Elevation of the lowest point	Left water edge	Right water edge
1	826.10	812.9	18	318
2	826.77	811.0	44	756
3	826.89	814.5	633	827
4	827.25	814.3	555	1109
5	827.45	816.3	540	1075
6	827.53	816.2	502	1247
7	828.11	817.6	217	742

convergence criterion is satisfied.

3.3. Interpolating the elevation of the streamlines

The elevations of the vertices along the streamlines are interpolated from the nearest cross-sections, as shown in Fig. 3 for cross-sections 1 and 2. Points D and F are the intersections between a streamline and two cross-sections, and point E is a vertex along the streamline. The elevation of points D, E and F are denoted by $Z_{i,j}^{s1}$, $Z_{i,j+2}^{s(1,2)}$ and $Z_{i,j+n}^{s2}$, respectively, where i refers to the i^{th} streamline across the river, and j refers to the j^{th} vertices along the streamline. The superscripts $s1$ and $s2$ denote the measured cross-sections 1 and 2, respectively. The curved distances from point E to points D and F are denoted by $L_{j+2,j}$ and $L_{j+2,j+n}$, respectively. The elevations of points D and F can be simply interpolated using the measured cross-sections, and the distance can be easily calculated. Thus, the elevation of point E is determined by the distance from the vertices to the two cross-sections, and can be written as

$$Z_{i,j+2}^{s(1,2)} = Z_{i,j}^{s1} + \frac{L_{j+2,j}}{L_{j+2,j} + L_{j+2,j+n}} \left(Z_{i,j}^{s1} - Z_{i,j+n}^{s2} \right) \tag{12}$$

The interpolated streamlines are then integrated with the topographic data in the floodplain, which can be derived from the elevation points and contour lines. The entire river terrain model, including both the river channel and floodplain, is represented by a triangular irregular network, which is a commonly-used geographic information system (GIS) technique to set up a terrain model, and can use multiple data forms, such as points, contour lines, or polygons (Zeiler, 2010).

4. Application

4.1. Study area

The proposed method to reconstruct the river terrain is applied and validated for the Shuibeicun reach in the Qinhe River, which is located in the middle of the Yellow River Basin, China (Fig. 4). As a railway bridge will be built in this reach, the lowest elevation of the bridge must be evaluated to ensure that a one-hundred-year flood can pass under the bridge. To calculate the elevation of the design flood, the two-dimensional numerical model will be applied, so that the river terrain must first be created.

Here we present a method that uses remote sensing images to identify the boundaries of the thalweg and the water edge, which are then applied to generate two types of streamlines. This paper generates two types of streamlines by selecting the water edge or thalweg boundaries and interpolates three river terrain models with different resolution. To analyze the error of the three reconstructed river terrain models, measured cross-sections are compared with the interpolated ones. The two-dimensional shallow-water equations are then applied to calculate the flood extent and depth.

4.2. Identification of the boundary of the water edge and the thalweg

Fig. 5 shows the available data, including the water edge, the thalweg and seven measured cross-sections, which were obtained using different methods. The elevations and locations of the cross-sections were measured using a total station instrument in September 2015.

The thalweg was identified based on remote sensing images and the measured cross-sections. Since the cross-sections were obtained in September 2015, a Landsat 8 remote image of 30-m resolution with 12 bands (Loveland and Irons, 2016) was selected on September 26 to detect the thalweg. To observe the body of water, the 5^{th}, 6^{th} and 4^{th} bands are composited into a single image, corresponding to the bands of near infrared, red and short-wave infrared light, respectively. The combination of the three bands transfers the color of land and water bodies into green and blue, respectively, and is an effective way to identify water bodies on a riverine floodplain. The result of the multiband composite image is shown in Fig. 5, where an obvious water body can be observed. In September 2015, the discharge of the Shuibeicun reach was about 30 m^3/s and the width of the river was less than 50 m. Furthermore, some of the lowest points from the measured cross-sections (Table 1) represent the location of the thalweg. Finally, the thalweg line can be fitted with a spline function (e.g (De Boor, 2001).), which passes through the lowest points and within the confines of the water body.

The water edge was identified from the solution of the one-dimensional open-channel equations (e.g (Chow, 2009).) and the measured contour lines. An ideal water edge line is the boundary during the time of bankfull discharge, which is the best condition for generating the streamlines. In this situation, the channel is full of water without

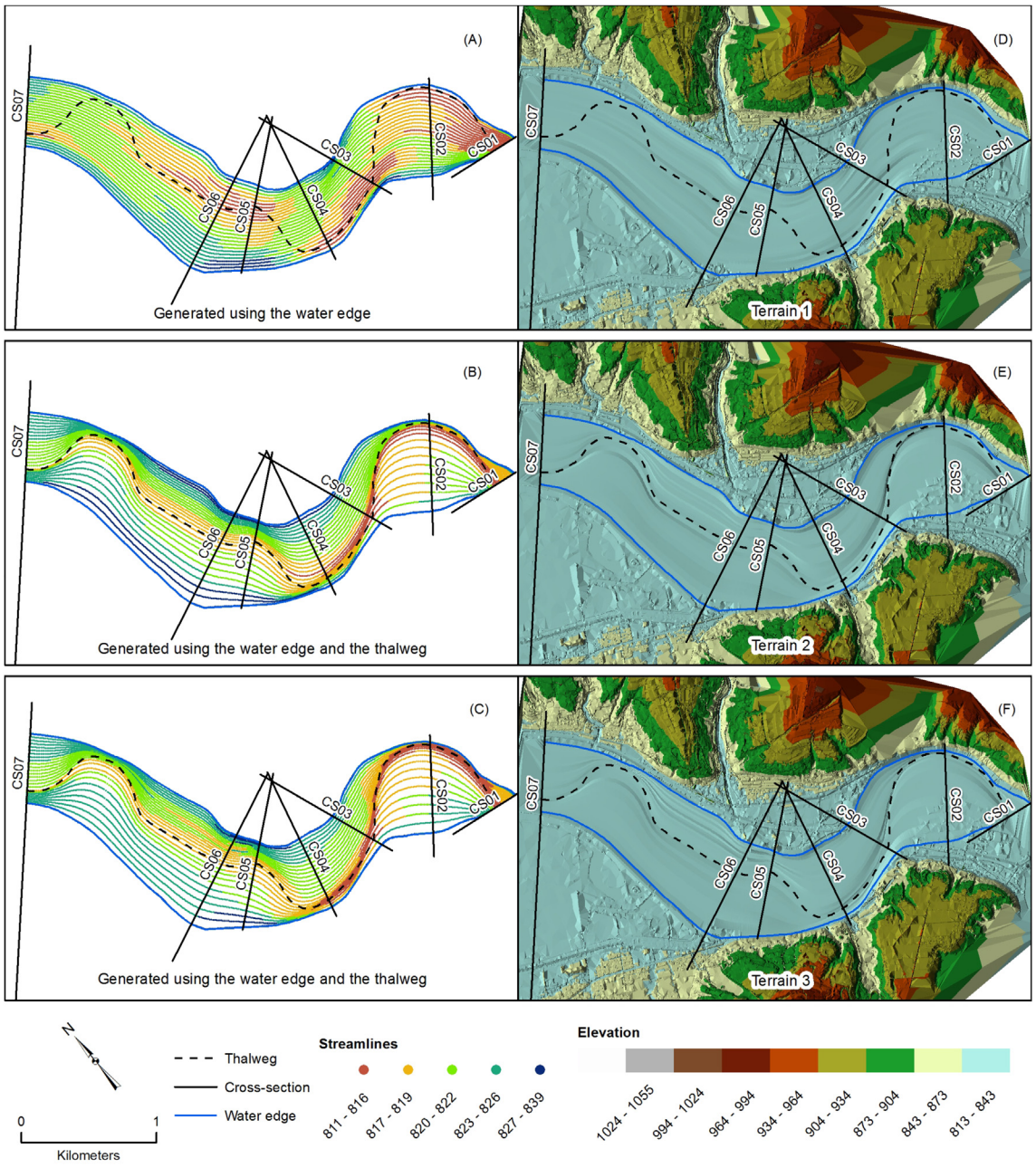

Fig. 6. Results of the generated river terrain.

overflowing the banks, and has a maximum area of wettable cross-section. While the water edge should normally be obtained from field measurements, in most cases, it is difficult to obtain this line in conditions of bankfull discharge.

One solution is to solve the one-dimensional open-channel model to calculate the water surface profile and identify its intersection points at the geometric shape of the measured cross-sections. These intersection points are then used as key points to control the shape of the water edge lines.

The solution of the one-dimensional open-channel model requires two boundary conditions. One condition is the bankfull discharge of this reach, which is considered as the input discharge, and is estimated using the rating curve of cross-section 1, which also corresponds to the outlet of the domain. The rating curve is the relationship between the discharge and the water level, and can be statically calculated using historical observational data. According to the rating curve of cross-section 1, the bankfull discharge is 6500 m^3/s when the geometry of its cross-section is considered. The second boundary condition is the roughness value. Empirically, the roughness is 0.032 in the main channel and 0.035 in the floodplain area for this reach.

Table 1 shows the derived water-surface profile and the locations of the intersection points between the seven cross-sections and the water-surface profile, which decreases from 828.11 m at cross-section 7–826.10 m at cross-section 1. The intersection between the profile and the cross-sections is measured from the left bank.

The shape of the water edge lines can be fitted with a spline function, which passes through these intersection locations and follows the foot of the mountain observed from the measured contour lines.

4.3. Result of the created river channel

To assess the error of the recreated terrain, three river terrain models with different boundary conditions were generated by the interpolation described above. The streamlines of terrain 1 are generated from the

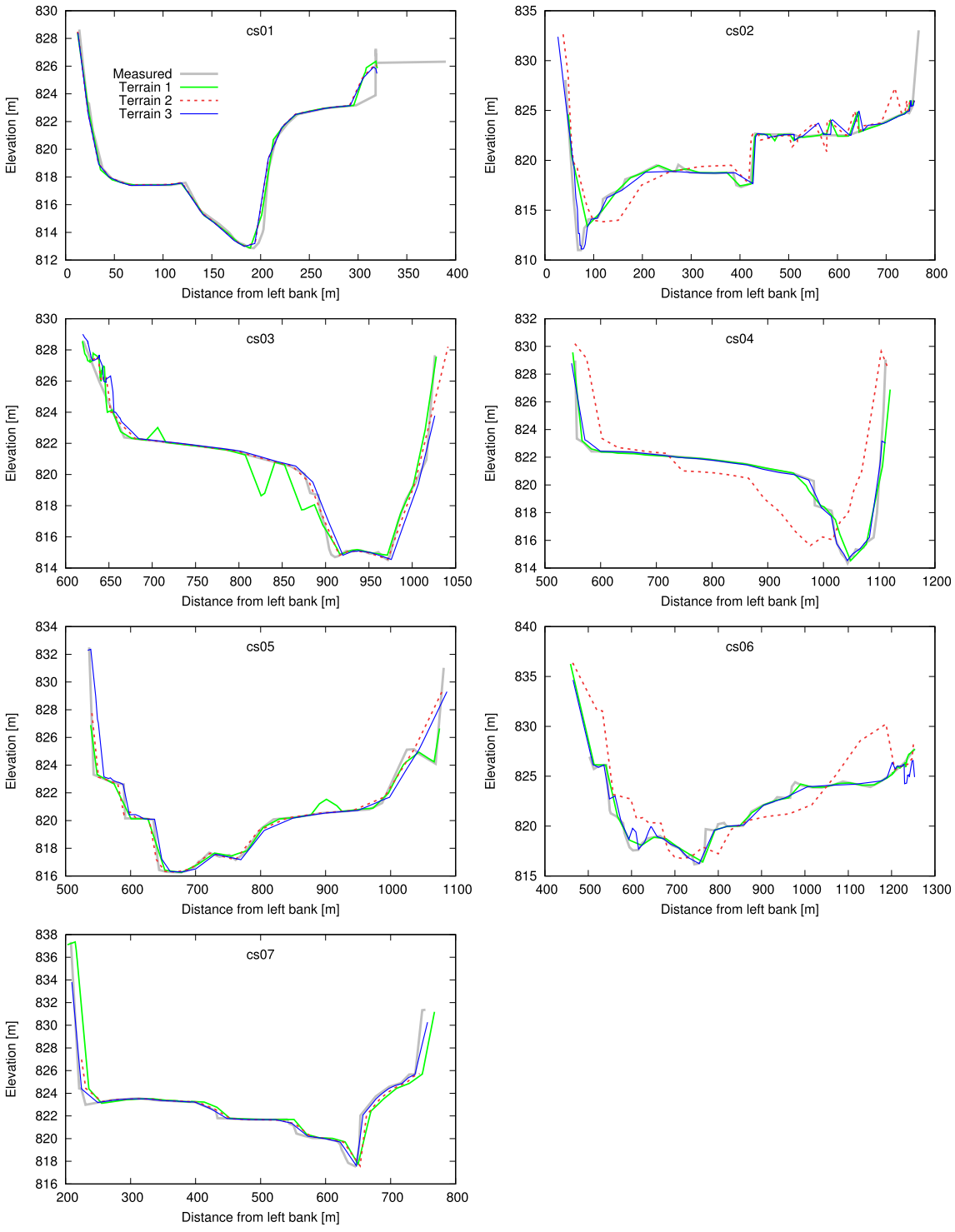

Fig. 7. Comparison of cross-sections derived from the generated channel with measured cross-sections.

thalweg and interpolated using all seven measured cross-sections. Terrain 2 uses the boundary of the thalweg and the water edge to generate the streamlines, but interpolated using selected cross-sections 1, 3, 5 and 7. For terrain 3, the boundaries applied to generate the streamlines are same as terrain 2, but all the seven measured cross-sections are used for the interpolation. For the three types of river terrain models, the contour lines of the floodplain area are the same. The algorithm was performed using the GCC Fortran compiler installed on a Linux Ubuntu 16.04 operating system. The computational time to generate the streamlines takes several minutes.

The results of the generated streamlines are shown in Fig. 6. For terrain 1 (Fig. 6(A)), the generated streamlines are spread uniformly along the river channel because only the water edge lines were considered. For terrains 2 and 3 (Fig. 6(B) and (C)), the thalweg line divides the streamlines into two, with 18 and 10 streamlines toward the left and right banks, respectively, and the distance between adjacent streamlines changes with the geometry of the river. In other words, a smaller distance between the thalweg and the water edge lines corresponds to a smaller distance between the two nearest streamlines, and vice versa. As the separation of the thalweg from the water edge at the concave bank is

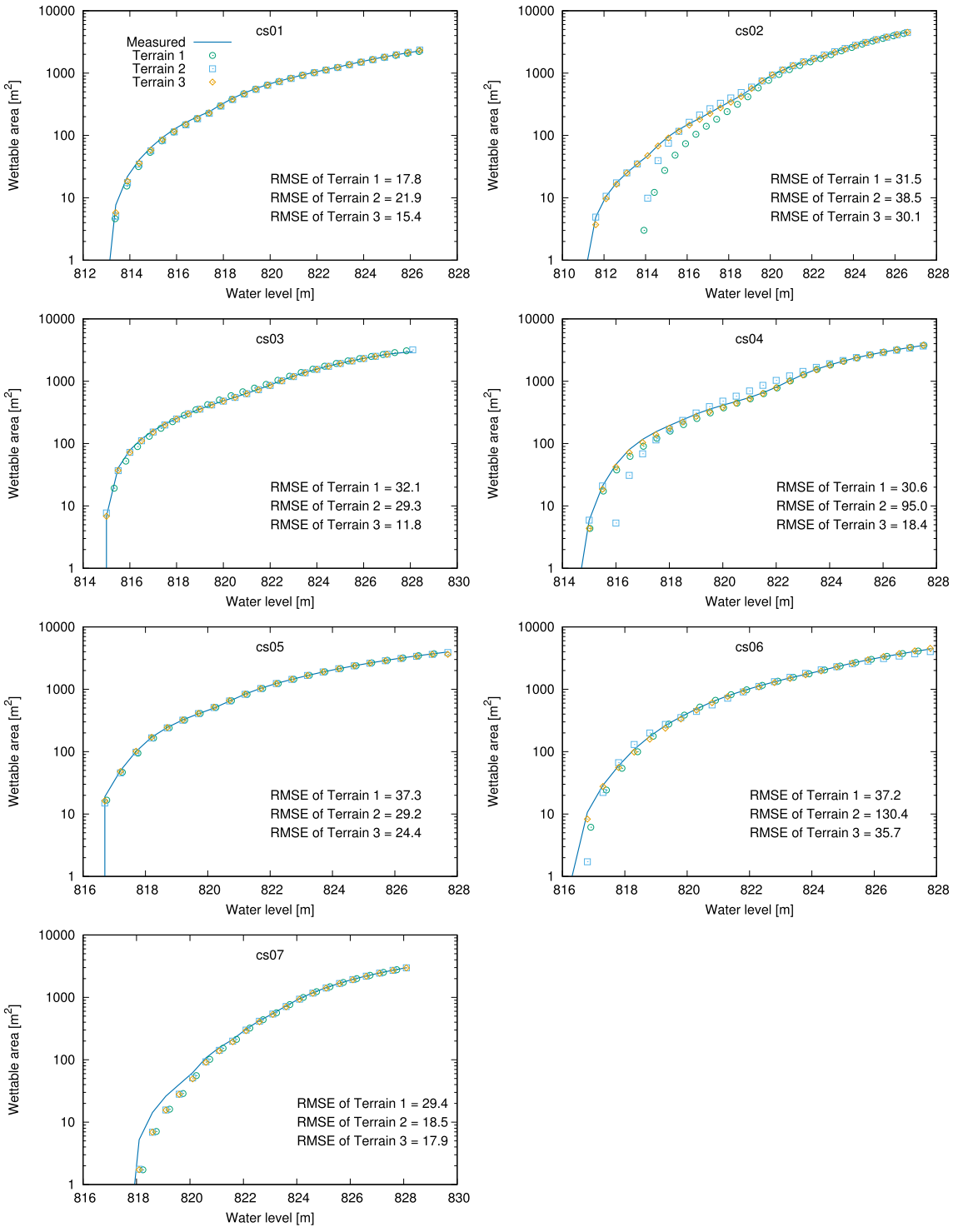

Fig. 8. The variation of the wettable cross-sectional area with the increase of water level.

normally smaller than that for the convex bank in natural rivers, more streamlines must be created at the concave bank to describe the gradient of the terrain. Along each streamline, the average distance between the nearest vertices is 10 m, and the vertices are sufficiently dense to reconstruct the change in the river channel.

For terrain 1, the interpolated elevations along the thalweg are not very smooth, especially at cross-sections 3 and 5, and even change sharply. For terrains 2 and 3, however, the elevations along the thalweg are smooth and change gradually.

Fig. 6(D), (E), (F) shows the interpolated results of the three terrain models, respectively, where, except for terrain 1, a distinct river channel along the thalweg is observed.

4.4. Validation using the measured cross-sections

The interpolated river terrain models are validated using the measured cross-sections in terms of the geometrical shape and the wettable area of the cross-section for a given water level.

Fig. 7 compares the interpolated geometry of the three terrain models with the measurements. For terrain 1, where only the water edge lines

Table 2
Cases for the two-dimensional numerical models.

Case name	Terrain	Discharge (m^3/s)
$Case_{T1}^{100}$	Terrain 1	100
$Case_{T1}^{6500}$	Terrain 1	6500
$Case_{T2}^{100}$	Terrain 2	100
$Case_{T2}^{6500}$	Terrain 2	6500
$Case_{T3}^{100}$	Terrain 3	100
$Case_{T3}^{6500}$	Terrain 3	6500

are used to generate the streamlines, the geometry of interpolated cross-sections looks reasonable, except for cross-sections 2, 3 and 5. The elevations of cross-section 3 and 5 change sharply, because the spread of the streamlines is inconsistent with the path of the thalweg.

For terrain 2, except for cross-sections 1, 3, 5 and 7, the generated cross-sections 2, 4 and 6 have different geometries from the measurements. As the elevation of the interpolated streamlines can only be controlled by the selected cross-sections, the channel morphology of cross-sections 2, 4 and 6 is difficult to recreate. Taking cross-section 2 as an example, Table 1 shows that the elevation of the lowest point drops from 812.9 m at cross-section 1–811.0 m at cross-section 2, and then increases to about 814 m at cross-sections 3 and 4. The capture of the sharp change of the bed elevation at cross-section 2 is difficult because only the selected cross-sections 1 and 3 are used for the interpolation. Thus, the shapes of the cross-sections for terrain 2 are poorly generated.

As terrain 3 incorporates both the water edge and the thalweg lines in the generation of the streamlines, and all the measured cross-sections are used for the interpolation, the overall shape of the terrain looks reasonable and significantly improved over the other terrain models.

Therefore, when more measurements are used, the shape of the cross-section has a higher quality. Moreover, the generated cross-sections perform better for gradual changes of the channel bed without any abrupt decrease or increase.

The results of the wettable area of the cross-section at a given water

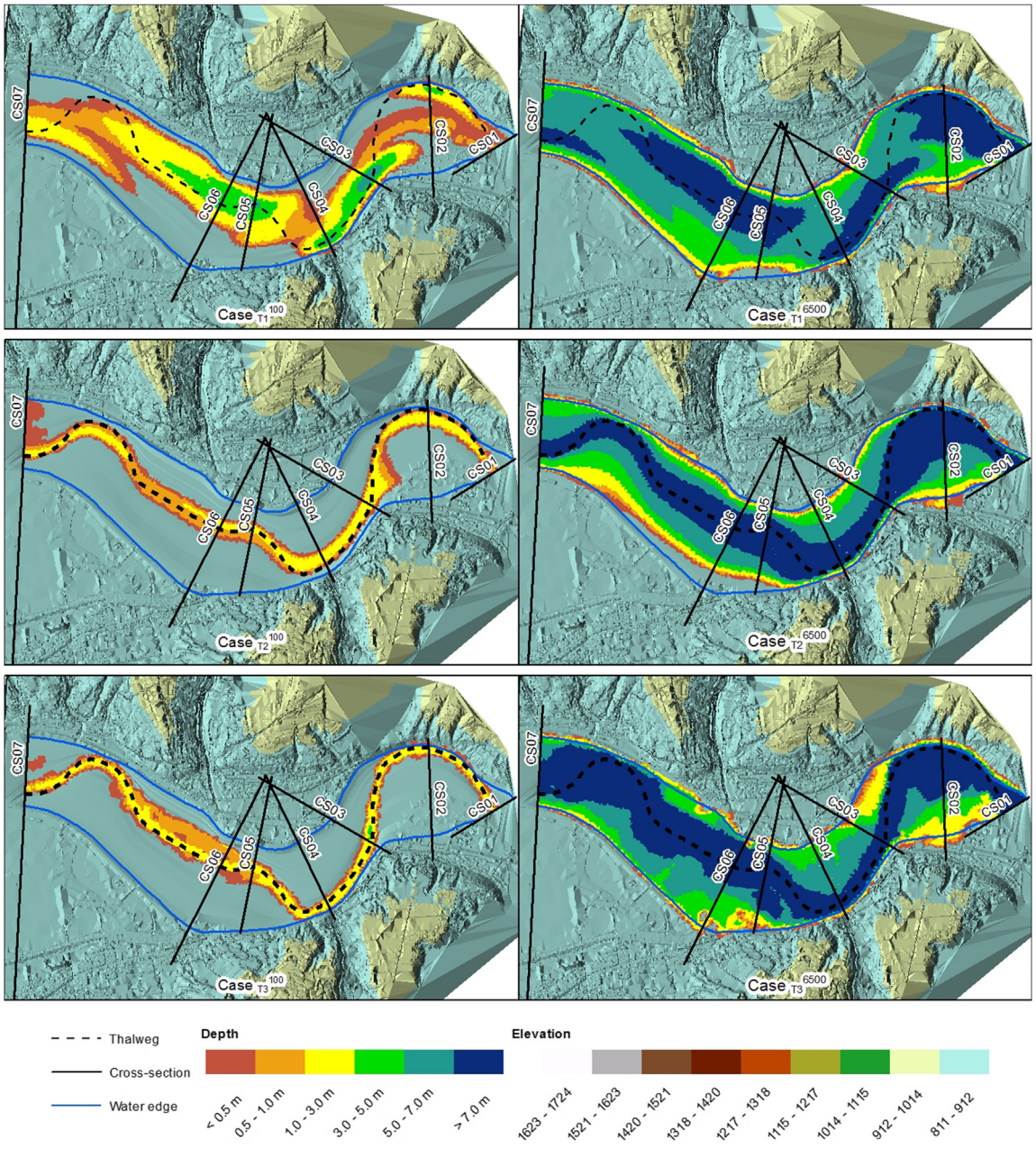

Fig. 9. Flood extent and depth as calculated from the two-dimensional shallow-water equations.

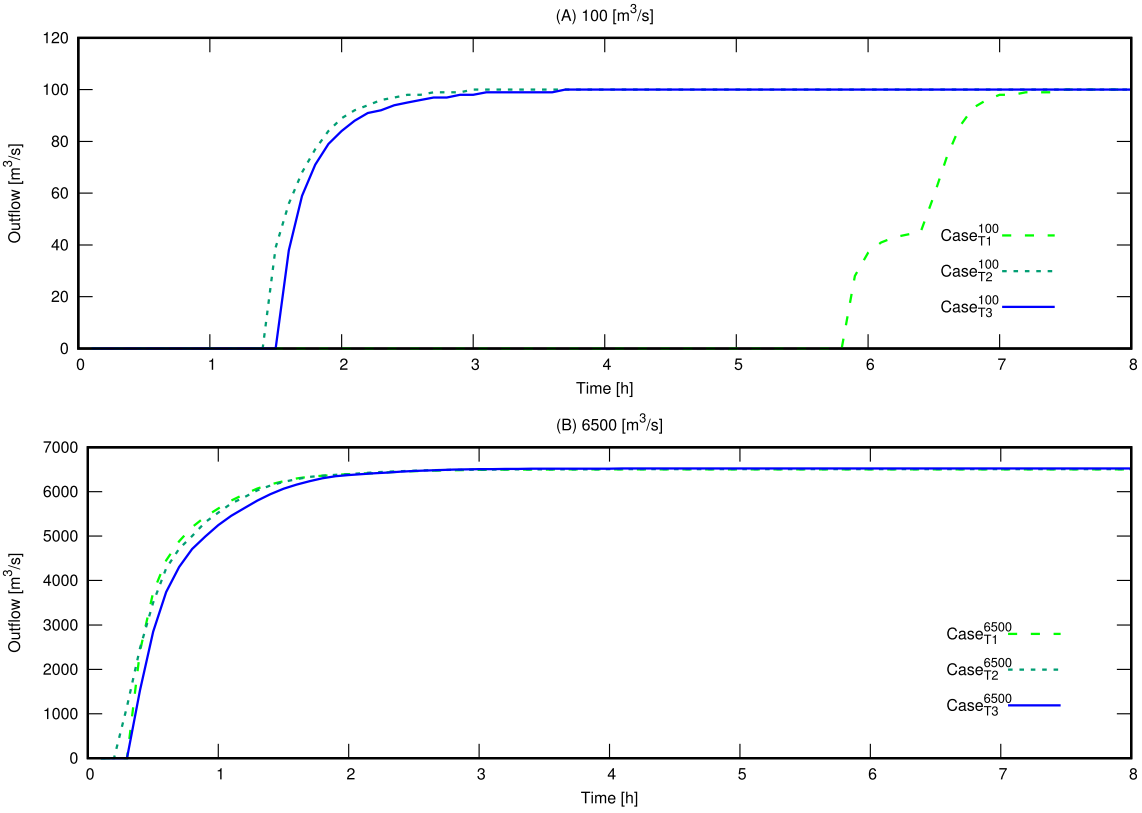

Fig. 10. Simulated flood outflow hydrographs.

level are given in Fig. 8, with the errors between the measured and interpolated data defined by the root-mean-square error (RMSE), whereby the RMSE for terrain 1 is smaller than for terrain 2, and terrain 3 gives the lowest RMSE error.

For terrain 2, the cross-sections 2, 4, 6 have increasing RMSE with the increase of water level. Specifically, for cross-section 4, the values of wettable area under the water level of 819 m are smaller than the value from the measured cross-section, implying that the wettable area for this cross-section is underestimated, and, at that water level, a smaller value of discharge is able to pass through the cross-section. If this cross-section were to be used to build up the two-dimensional hydrodynamic model, the calculated water level would be larger than the actual value. The cross-section 7 generated by all three terrain models for the water level of 821 m would have similar effects.

4.5. Results of the two-dimensional simulations

The two-dimensional shallow-water equations (e.g. (Anastasiou and Chan, 1997) (Begnudelli and Sanders, 2006);) are applied to evaluate the performance of the three terrain models. The lack of observations of historical floods means that two design cases of the steady discharge, $100m^3/s$ and $6500m^3/s$, are used for the calculation of the flood extent and depth. The low flow rate ($100m^3/s$) is sufficiently small to test whether the created channel is smooth, particularly in the area of the main channel. The higher flow rate ($6500m^3/s$) is considered to be the bankfull discharge, and is identical to the value used to identify the boundary of the water edge. The cases designed for testing are listed in Table 2.

The finite-volume method is used to discretize the two-dimensional shallow-water equations for a set of 33,000 triangular cells (e.g., (Lai et al., 2013) (Lu and Xie, 2016);). The size of these cells in the main channel is about 20 m, but 30 m in the floodplain area. The initial conditions, such as the roughness, are identical to those defined in Section 4.2.

Fig. 9 shows the calculated flood extent and depth. For the low discharge rate ($100m^3/s$), the flood extent of Case_{T1}^{100} is clearly larger than Case_{T2}^{100} and Case_{T3}^{100}. As shown in Fig. 6, the terrain 1 is not smooth along the main channel. For this reason, although there is a low discharge rate, the flooding would occur over low terrain, resulting in a larger flood extent. Compared with Case_{T1}^{100}, Case_{T2}^{100} and Case_{T3}^{100} have a similar and more realistic flood extent. It is clear that the position of the thalweg in the latter two cases is always at the center of the river, although the flood extent of Case_{T3}^{100} from cross-sections 6 to 7 is slightly larger than the results from Case_{T2}^{100}. The difference can be explained from the geometry of the interpolated cross-sections shown in Fig. 7. By comparing these results with the measurements of cross-section 6, especially at the left bank from 500 m to 750 m, terrain 3 obtains a more reasonable geometric shape than that for terrain 2. As a result, the interpolated elevation from cross-section 6 to 7 for terrain 3 should be lower than that for terrain 2, so that the results of the flood extent for Case_{T3}^{100} are more reasonable than that for Case_{T2}^{100}.

For the higher discharge rate ($6500m^3/s$), all the three terrain models result in a similar flood extent. Especially for Case_{T3}^{6500}, the flood extent and water edge line have almost identical shapes, where the water edge is the boundary of the bankfull discharge. The calculated flood extent from the two-dimensional hydrodynamic model fits well with the water edge lines calculated using the one-dimensional open channel model. Therefore, we conclude that the reconstructed river terrain has a reasonable volume to accommodate the higher discharge.

Fig. 10 shows simulated dry-to-steady outflow hydrographs for the six cases. For Case_{T2}^{100} and Case_{T3}^{100}, the arrival time of the flood to outlet (cross-section 1) takes approximately 1.5 h. In contrast, the arrival time for Case_{T1}^{100} takes more than 5.5 h, which follows from the poorly generated terrain for this case, resulting in the flood extent over a larger area, and the delay of the arrival time at the outlet. For the higher discharge rate ($6500m^3/s$), the arrival time for the three cases is similar (0.5 h), with the time to steady state of about 3 h.

5. Conclusions

An accurate geometric description of the main channel bathymetry and floodplain along a river is important for yielding reliable results from hydrodynamic numerical models, the ability to understand the characteristics of a river, such as the flow and bedform, and assessing their interaction with engineering applications. However, in most cases, a river terrain model, particularly for the area under the water body, is difficult to acquire, and there are a lack of available data describing the geometry of the river channel.

We present an algorithm to generate a continuous river channel by interpolation of measured cross-sections. Our algorithm, which is based on the idea of grid generation for computational fluid dynamics, solves a simple elliptic partial differential equation to generate the streamlines of the river channel. The elevations of the vertices on the streamlines are calculated twice. The entire river terrain is integrated with the surrounding topography, such as the elevation points or contour lines. The proposed method has been applied and validated for the Qinhe River in the middle of the Yellow River Basin, China. Three river terrain models with different resolutions are interpolated using different types of boundary lines and selected cross-sections. Cross-sectional validation was used to test the error of the geometrical shape of the created river channel. The two-dimensional shallow-water equations are also studied for two discharge rates to calculate the flood extent and depth of the three terrain models.

Our results show that the generated streamlines correspond well with the boundaries of the water edge and the thalweg when constrained by the elliptic partial differential equations, and are smooth when transformed from a computational domain with regularly calculated grid lines. The benefits of these created streamlines include their ability to maintain a consistent shape of the interpolated cross-sections with the measurements, and to enforce smoothness of the main channel.

Validation shows that if enough measurements of cross-sections are used, the shapes of the interpolated cross-sections are consistent with the measurements. The results indicate that both the water edge and the thalweg are important boundary conditions for the generation of a reasonable terrain model. The results from the two-dimensional shallow-water equations indicate that, if the thalweg line is applied in the interpolated river terrain model, a better flood extent and depth is obtained. As evidenced by the results of the low discharge rate (100 m^3/s) for Case_{T2}^{100} or Case_{T3}^{100}, the interpolated river channel is very smooth. In addition, the calculated flood extent for Case_{T3}^{6500} corresponds well with the water edge lines calculated using the one-dimensional open channel model, which indicates that the reconstructed river terrain has a reasonable volume for a higher discharge rate.

Although our algorithm performs well, it can only be used for a single channel. In future work, more exhaustive measurements should be applied to improve the accuracy of the method. Furthermore, complicated geomorphologies, such as islands and confluences, must be addressed to make the work more applicable.

Acknowledgments

This work was partially funded and supported by the National Natural Science Foundation of China (Grant Nos. 51409113 and 51479081), the National Key Research and Development Program (2016YFC0402409-07), and the Key Laboratory of Water Science and Engineering, Nanjing Hydraulic Research Institute (YK914002).

References

Anastasiou, K., Chan, C.T., 1997. Solution of the 2d shallow water equations using the finite volume method on unstructured triangular meshes. Int. J. Numer. Meth. Fluids 24 (11), 1225–1245. https://doi.org/10.1002/(SICI)1097-0363(19970615)24:11<1225::AID-FLD540>3.0.CO;2-D.

Anderson, J.D., 1995. Computational Fluid Dynamics: the Basics with Applications. McGraw-Hill Series in Mechanical Engineering, McGraw-Hill, New York.

Bailly du Bois, P., 2011. Automatic calculation of bathymetry for coastal hydrodynamic models. Comput. Geosci. 37 (9), 1303–1310. https://doi.org/10.1016/j.cageo.2010.11.018.

Begnudelli, L., Sanders, B.F., 2006. Unstructured grid finite-volume algorithm for shallow-water flow and scalar transport with wetting and drying. J. Hydraul. Eng. 132 (4), 371–384. https://doi.org/10.1061/(ASCE)0733-9429(2006)132:4(371).

Caviedes-Voullime, D., Morales-Hernndez, M., Lpez-Marijuan, I., Garca-Navarro, P., 2014. Reconstruction of 2d river beds by appropriate interpolation of 1d cross-sectional information for flood simulation. Environ. Model. Softw. 61, 206–228. https://doi.org/10.1016/j.envsoft.2014.07.016.

Chow, V.T., 2009. Open-channel Hydraulics. Blackburn Press, Caldwell, NJ.

Colbo, K., Ross, T., Brown, C., Weber, T., 2014. A review of oceanographic applications of water column data from multibeam echosounders. Estuar. Coast. Shelf Sci. 145, 41–56. https://doi.org/10.1016/j.ecss.2014.04.002.

Costa, B., Battista, T., Pittman, S., 2009. Comparative evaluation of airborne LiDAR and ship-based multibeam SoNAR bathymetry and intensity for mapping coral reef ecosystems. Remote Sens. Environ. 113 (5), 1082–1100. https://doi.org/10.1016/j.rse.2009.01.015.

De Boor, C., 2001. A Practical Guide to Splines, Rev. Ed Edition, No. V. 27 in Applied Mathematical Sciences. Springer, New York.

Fletcher, C.A.J., Srinivas, K., 1991. Computational Techniques for Fluid Dynamics, second ed. Springer Series in Computational Physics, Springer-Verlag, Berlin ; New York.

Hardy, R.J., Bates, P.D., Anderson, M.G., 1999. The importance of spatial resolution in hydraulic models for floodplain environments. J. Hydrol. 216 (1–2), 124–136.

Horritt, M., Bates, P., Mattinson, M., 2006. Effects of mesh resolution and topographic representation in 2d finite volume models of shallow water fluvial flow. J. Hydrol. 329 (1–2), 306–314. https://doi.org/10.1016/j.jhydrol.2006.02.016.

Intelmann, S.S., Aug. 2006. Comments on Hydrographic and Topographic LIDAR Acquisition and Merging with Multibeam Sounding Data Acquired in the Olympic Coast National Marine Sanctuary. Tech. Rep. ONMS-06–05, U.S. Department of Commerce, Silver Spring, Maryland.

Jansen, P.P. (Ed.), 1979. Principles of River Engineering: the Non-tidal Alluvial River. Pitman, London ; San Francisco.

Knabner, P., Angermann, L., 2003. Numerical Methods for Elliptic and Parabolic Partial Differential Equations, No. 44 in Texts in Applied Mathematics. Springer, New York.

Lai, X., Jiang, J., Liang, Q., Huang, Q., 2013. Large-scale hydrodynamic modeling of the middle Yangtze River Basin with complex riverlake interactions. J. Hydrol. 492, 228–243. https://doi.org/10.1016/j.jhydrol.2013.03.049. http://linkinghub.elsevier.com/retrieve/pii/S0022169413002771.

Leopold, L.B., Wolman, M.G., 1957. River Channel Patterns: Braided, Meandering and Straight. Tech. Rep. 282–B. US Geological Survey.

Li, J., Heap, A.D., 2011. A review of comparative studies of spatial interpolation methods in environmental sciences: performance and impact factors. Ecol. Inf. 6 (3–4), 228–241. https://doi.org/10.1016/j.ecoinf.2010.12.003.

Li, Z., Zhu, Q., Gold, C., 2005. Digital Terrain Modeling: Principles and Methodology. CRC Press, New York.

Loveland, T.R., Irons, J.R., 2016. Landsat 8: the plans, the reality, and the legacy. Remote Sens. Environ. 185, 1–6. https://doi.org/10.1016/j.rse.2016.07.033. http://linkinghub.elsevier.com/retrieve/pii/S0034425716302905.

Lu, X., Xie, S., 2016. Conventional versus pre-balanced forms of the shallow-water equations solved using finite-volume method. Ocean. Model. 101, 113–120. https://doi.org/10.1016/j.ocemod.2016.04.002. http://linkinghub.elsevier.com/retrieve/pii/S1463500316300075.

Marie Morisawa, K., Clayton, M., 1985. Rivers: Form and Process, No. 7 in Geomorphology Texts. Longman, London ; New York.

Merwade, V.M., Maidment, D.R., Hodges, B.R., 2005. Geospatial representation of river channels. J. Hydrol. Eng. 10 (3), 243–251. https://doi.org/10.1061/(ASCE)1084-0699(2005)10:3(243).

Merwade, V., Cook, A., Coonrod, J., 2008. GIS techniques for creating river terrain models for hydrodynamic modeling and flood inundation mapping. Environ. Model. Softw. 23 (10–11), 1300–1311. https://doi.org/10.1016/j.envsoft.2008.03.005.

Morisawa, Marie, 1968. Streams Their Dynamics and Morphology, Earth and Planetary Science Series. McGraw-Hill, New York.

Nittrouer, J.A., Allison, M.A., Campanella, R., 2008. Bedform transport rates for the lowermost Mississippi River. J. Geophys. Res. 113 (F3) https://doi.org/10.1029/2007JF000795.

Petersen, M.S., 1986. River Engineering. Prentice-Hall, Englewood Cliffs, N.J.

Podhornyi, M., Unucka, J., Bobl, P., hov, V., 2013. Effects of LIDAR DEM resolution in hydrodynamic modelling: model sensitivity for cross-sections. Int. J. Digital Earth 6 (1), 3–27. https://doi.org/10.1080/17538947.2011.596578.

Raber, G.T., Jensen, J.R., Hodgson, M.E., Tullis, J.A., Davis, B.A., Berglund, J., 2007. Impact of lidar nominal post-spacing on DEM accuracy and flood zone delineation. Photogramm. Eng. Remote Sens. 73 (7), 793–804. https://doi.org/10.14358/PERS.73.7.793.

Schppi, B., Perona, P., Schneider, P., Burlando, P., 2010. Integrating river cross section measurements with digital terrain models for improved flow modelling applications. Comput. Geosci. 36 (6), 707–716. https://doi.org/10.1016/j.cageo.2009.12.004.

Thompson, J.F., Thames, F.C., Mastin, C.W., 1977. Boundary-fitted Curvilinear Coordinate Systems for the Solution of Partial Differential Equations on Fields

Containing Any Number of Arbitrary Two-dimensional Bodies. Tech. Rep. NASA CR-2729, NASA, Mississippi State University.
Thompson, J.F., Warsi, Z.U.A., Mastin, C.W., 1985. Numerical Grid Generation: Foundations and Applications. North-Holland. Elsevier Science Pub, New York. Co. [distributor].
Vogel, S., Mrker, M., 2010. Reconstructing the roman topography and environmental features of the sarno river plain (Italy) before the AD 79 eruption of SommaVesuvius. Geomorphology 115 (1–2), 67–77. https://doi.org/10.1016/j.geomorph.2009.09.031.
Zeiler, M., 2010. Modeling Our World: the ESRI Guide to Geodatabase Concepts, second ed. ESRI Press, Redlands, Calif.